

RESEARCH PAPER

## Hydrothermal Synthesis, Characterization and Catalytic Performance of La<sup>3+</sup> and Sm<sup>3+</sup> - Doped Bi<sub>2</sub>Mn<sub>2</sub>O<sub>7</sub> Nanocatalysts for Biginelli Reactions

Shahin Khademinia and Mahdi Behzad\*

Department of chemistry, Semnan University, Semnan, Iran

### ARTICLE INFO

**Article History:**

Received 08 October 2018

Accepted 14 November 2018

Published 01 January 2019

**Keywords:**

Biginelli

Hydrothermal

Lanthanum; Nanocatalysts;

Pyrochlores

Samarium

### ABSTRACT

La<sup>3+</sup> and Sm<sup>3+</sup> - doped Bi<sub>2</sub>Mn<sub>2</sub>O<sub>7</sub> nanocatalysts were synthesized in 1 M NaOH aqueous solution, via a stoichiometric 1:1 Bi:Mn molar ratio hydrothermal method at 180 °C for 48 h. Bi(NO<sub>3</sub>)<sub>3</sub>, MnO<sub>2</sub>, La(NO<sub>3</sub>)<sub>3</sub> and Sm<sub>2</sub>O<sub>3</sub> were used as raw materials. The synthesized nanomaterials were characterized by powder X-ray diffraction (PXRD) technique. Both of the La<sup>3+</sup> and Sm<sup>3+</sup> - doped Bi<sub>2</sub>Mn<sub>2</sub>O<sub>7</sub> nanomaterials were crystallized in a cubic crystal structure with space group . The morphologies of the synthesized materials were studied by field emission scanning electron microscope (FESEM). The optical properties of the as-synthesized nanomaterials were studied by ultraviolet visible (UV-Vis) diffuse reflectance spectra (DRS). It was found that the optical band gaps were increased with doping La<sup>3+</sup> and Sm<sup>3+</sup> into Bi<sub>2</sub>Mn<sub>2</sub>O<sub>7</sub>. Catalytic performance of the synthesized nanomaterials were investigated in Biginelli reactions which showed excellent efficiency. Correlation between the catalytic performance with the band gap and hard/soft proportion of the metal ions was shown.

### How to cite this article

Khademinia S, Behzad M. Hydrothermal Synthesis, Characterization and Catalytic Performance of La<sup>3+</sup> and Sm<sup>3+</sup> - Doped Bi<sub>2</sub>Mn<sub>2</sub>O<sub>7</sub> Nanocatalysts for Biginelli Reactions. J Nanostruct, 2019; 9(1):172-182. DOI: 10.22052/JNS.2019.01.019

### INTRODUCTION

A<sub>2</sub>B<sub>2</sub>O<sub>7</sub> pyrochlore type materials (where A is a medium-large cation and B is an octahedrally coordinated, high-charge cation) with space group of can be described as a fluorite superstructure with O anions ordered around the A and B cations. These materials have been widely studied as ferroelectric and/or magnetic materials, ionic conductors, catalysts and radiation resistant materials [1-6]. Pyrochlore materials have attracted great interest due to their ability to form substituted and defective structures, permitting interesting physical properties [7-9]. Rare earth (RE) compounds have been extensively studied as potential laser host materials, oxygen ion conductors, and fluorescent lamp phosphors due to their attractive optical, electric, and magnetic properties, which are attributed to the electronic

\* Corresponding Author Email: [mbehzad@semnan.ac.ir](mailto:mbehzad@semnan.ac.ir)

transitions of rare earth ions between the 4f energy levels [10–13]. In the RE family, Sm<sup>3+</sup> is one of the most important active ions and can show intense line-like absorption bands for special infrared light because of its closely lying energy level structure [14]. In recent years, considerable efforts have been focused on the fabrication of ceramic materials and RE oxides [12–20]. Doping is expected to introduce defect and change in the lattice energy of the crystals. La<sub>2</sub>O<sub>3</sub> has also the greatest effect among the various additives in changing the lattice energy of crystals [21].

The Biginelli reaction was originally reported by Biginelli in 1891 [23]. It is a methodology for the synthesis of 3,4-dihydropyrimidin-2-(1H)-one derivatives (DHPMs) in a one-step procedure. DHPMs have shown several applications [24]. Several metal oxides have been reported as



This work is licensed under the Creative Commons Attribution 4.0 International License.

To view a copy of this license, visit <http://creativecommons.org/licenses/by/4.0/>.

nanocatalysts for the Biginelli reactions including  $\text{Bi}_2\text{V}_2\text{O}_7$  [6], alumina supported Mo catalysts [25], nano ZnO as a structure base catalyst [26],  $\text{MoO}_3\text{-ZrO}_2$  nanocomposite [27],  $\text{MnO}_2\text{-MWCNT}$  nanocomposites [28],  $\text{TiO}_2$  nanoparticles [29],  $\text{Mg-Al-CO}_3$  and  $\text{Ca-Al-CO}_3$  hydrotalcite [30],  $\text{Bi}_2\text{O}_3/\text{ZrO}_2$  nanocomposite [31],  $\text{ZrO}_2\text{-Al}_2\text{O}_3\text{-Fe}_3\text{O}_4$  [32], imidazole functionalized  $\text{Fe}_3\text{O}_4@\text{SiO}_2$  [33], Alumina supported  $\text{MoO}_3$  [34],  $\text{ZrO}_2$ -pillared clay [35], ZnO nanoparticle [36],  $\text{Fe}_3\text{O}_4\text{-CNT}$  [37],  $\text{TiO}_2\text{-MWCNT}$  [38],  $\text{Fe}_3\text{O}_4@\text{mesoporous SBA-15}$  [39],  $\text{Bi}_2\text{Mn}_2\text{O}_7$  [40] and  $\text{RuO}_2$  [41].

Recently we have reported the synthesis of the nanostructured  $\text{Bi}_2\text{Mn}_2\text{O}_7$  and  $\text{Bi}_2\text{V}_2\text{O}_7$ . The cooperative catalytic performance between the metal ions in the above mentioned materials have also been reported in Biginelli reactions [6, 40]. In continuation of our research on the effect of different factors on the cooperative catalysis of the Biginelli reaction, herein we report the synthesis of  $\text{La}^{3+}$  and  $\text{Sm}^{3+}$  - doped  $\text{Bi}_2\text{Mn}_2\text{O}_7$  with general formula  $\text{Bi}_{2-x}\text{La}_x\text{Mn}_2\text{O}_7$  and  $\text{Bi}_{2-x}\text{Sm}_x\text{Mn}_2\text{O}_7$  nanomaterials. To the best of our knowledge, there is no report on the synthesis of the  $\text{La}^{3+}$  and  $\text{Sm}^{3+}$ -doped  $\text{Bi}_2\text{Mn}_2\text{O}_7$  nanomaterials. Besides, there is no report on the catalytic application of the obtained materials in the Biginelli reaction and the investigation of the correlation of the dopant metal ions with the catalytic application. So, the doped nanomaterials were used as nanocatalyst in Biginelli reaction for the synthesis of various DHPMs and the expected cooperation was seen again. Besides, it was rationalized that the hard/soft natures of the metal ions would play important role in the catalytic activity of such catalysts.

## MATERIALS AND METHODS

### General remarks

All chemicals were of analytical grade, obtained from commercial sources, and used without further purification. Phase identifications were performed on a powder X-ray diffractometer D5000 (Siemens AG, Munich, Germany) using  $\text{CuK}\alpha$  radiation. The elemental analyses of the obtained materials were examined with a Philips XL30 scanning electron microscope (Philips, Amsterdam, Netherlands) equipped with an energy-dispersive X-ray (EDX) spectrometer. The morphologies of the obtained materials were examined with a field emission scanning electron microscope (Hitachi FE-SEM model

S-4160). The UV-Vis diffuse reflectance spectra of the samples were recorded using an Avantes Spectrometer model Avaspec-2048-TEC. Cell parameter refinement was reported by celref software version 3 (Laboratoire des Matériaux et du Génie Physique de l'École Supérieure de Physique de Grenoble). The purity of the DHPMs was checked by thin layer chromatography (TLC) on glass plates coated with silica gel 60 F254 using n-hexane/ethyl acetate mixture as mobile phase.

### Hydrothermal synthesis of $\text{Bi}_{2-x}\text{La}_x\text{Mn}_2\text{O}_7$

In typical synthetic experiment, 0.01, 0.02 or 0.03 mmol  $\text{La}(\text{NO}_3)_3$  ( $\text{Mw}=324.92 \text{ g mol}^{-1}$ ) was mixed respectively with 2.05, 2.04 or 2.03 mmol  $\text{Bi}(\text{NO}_3)_3 \cdot 5\text{H}_2\text{O}$  ( $\text{Mw}=485.07 \text{ g mol}^{-1}$ ) in 70 mL of hot aqueous solution of 1M NaOH. 2.06 mmol  $\text{MnO}_2$  ( $\text{Mw}=86.94 \text{ g mol}^{-1}$ ) was then added and the resulting mixture were transformed into 100 mL Teflon – lined stainless steel autoclaves. The autoclaves were sealed and heated at 180 °C for 48h. When the reactions were completed, the autoclaves were cooled down to room temperature by water immediately. The prepared powders were collected, washed with distilled water and dried at 110 °C for 20 min and the black powders of the target materials were obtained.

### Hydrothermal synthesis of $\text{Bi}_{2-x}\text{Sm}_x\text{Mn}_2\text{O}_7$

The nanomaterials were synthesized following a similar procedure as described for  $\text{Bi}_{2-x}\text{La}_x\text{Mn}_2\text{O}_7$  except 0.01, 0.02, 0.03 or 0.04 mmol  $\text{Sm}_2\text{O}_3$  ( $\text{Mw}=348.8 \text{ g mol}^{-1}$ ) were mixed respectively with 2.05, 2.04, 2.03 or 2.02 mmol  $\text{Bi}(\text{NO}_3)_3 \cdot 5\text{H}_2\text{O}$ .

### General procedure for the synthesis of DHPMs

In a typical procedure, a mixture of aldehyde (1 mmol), ethyl acetoacetate (1 mmol), urea (1.2 mmol) and 0.014 g of  $\text{La}^{3+}$  or  $\text{Sm}^{3+}$  - doped  $\text{Bi}_2\text{Mn}_2\text{O}_7$  were placed in a round-bottom flask under solvent free conditions. The suspension was stirred at 104 °C. The progress of the reaction was monitored by thin layer chromatography (TLC) [6:4 hexane:ethylacetate]. After completion of the reaction, the solid crude product was washed with deionized water to separate the unreacted raw materials. The precipitated solid was then collected and dissolved in ethanol to separate the solid catalyst. The filtrate was left undisturbed at room temperature to afford the crystals of the pure product.

## RESULTS AND DISCUSSIONS

### PXRD analysis

The crystal phases of the synthesized materials were examined by powder X-ray diffraction technique. Fig. 1 and 2 show the PXRD patterns of the La<sup>3+</sup> and Sm<sup>3+</sup> - doped Bi<sub>2</sub>Mn<sub>2</sub>O<sub>7</sub> nanomaterials. The measured powder XRD data are similar to those of the corresponding un-doped Bi<sub>2</sub>Mn<sub>2</sub>O<sub>7</sub> nanomaterial [22]. Fig. 1 shows the PXRD patterns of La<sup>3+</sup> - doped Bi<sub>2</sub>Mn<sub>2</sub>O<sub>7</sub>. It was found that with increasing the dopant amount to 0.03 mmol (S<sub>3</sub>), there were some impurity peaks corresponding to the La<sub>2</sub>O<sub>3</sub>. So, the doping limitation was 0 to 0.02 mmol of La<sup>3+</sup> and S<sub>2</sub> was used for EDX analysis. Excess mole percent concentration of the dopant agent in the reaction mixture, resulted in impurity peaks in the XRD pattern in Fig. 1c [42, 43]. The diffraction lines at 2θ ≈ 39, 46, 55, 60 and 64° are assigned by their peak positions to the excess La<sub>2</sub>O<sub>3</sub> [42, 43]. The X-ray diffraction data for La<sub>2</sub>O<sub>3</sub> were identified using the Joint Committee on Powder Diffraction Standards (JCPDS) file: 73-2141.

Fig. 2 shows the PXRD patterns of Sm<sup>3+</sup> - doped Bi<sub>2</sub>Mn<sub>2</sub>O<sub>7</sub>. It was clear that with increasing the dopant amount to 0.04 mmol, some impurity peaks correspond to Sm<sub>2</sub>O<sub>3</sub> were detected. So, the doping limitation was 0 to 0.03 mmol of Sm<sup>3+</sup> and S<sub>5</sub> was used for EDX analysis. The excess amount of the dopant was appeared as impurity peaks in the XRD pattern of Fig. 1d [44, 45]. The diffraction lines at 2θ ≈ 35, 36, 47, and 63° are assigned by their peak positions to Sm<sub>2</sub>O<sub>3</sub> [44, 45].

Table 1 shows the interplanar spacing (d) data calculated from Bragg's equation for pure and La<sup>3+</sup> and Sm<sup>3+</sup> - doped Bi<sub>2</sub>Mn<sub>2</sub>O<sub>7</sub> nanomaterials. It was found that the d values were increased with increasing the dopant amount of La<sup>3+</sup> and Sm<sup>3+</sup> into Bi<sub>2</sub>Mn<sub>2</sub>O<sub>7</sub>. Besides, table 1 shows the cell parameter refinement data of the as-synthesized nanomaterials with standard deviation (SD) data for each sample. It was found that the cell parameters values were increased with increasing the dopant amounts. However, when doping the ions into the crystal system, the d and a values for S<sub>2</sub> and S<sub>3</sub> were decreased.

Table 2 shows the crystal sizes of the as-synthesized nanomaterials in different dopant concentrations calculated by Scherrer equation:

$$t = \frac{k\lambda}{B_{1/2} \cos \theta} \quad (1)$$

In this equation, t is the entire thickness of the crystalline sample, λ is the X-ray diffraction wavelength (0.154 nm), and k is the Scherrer constant (0.9), B<sub>1/2</sub> of FWHM is the full width at half its maximum intensity and θ is the half diffraction angle at which the peak is located. The data mentioned in table 2 shows that with doping La<sup>3+</sup> into Bi<sub>2</sub>Mn<sub>2</sub>O<sub>7</sub>, the crystal sizes were increased compared to pure Bi<sub>2</sub>Mn<sub>2</sub>O<sub>7</sub> nanomaterial. It was found that with doping Sm<sup>3+</sup> into Bi<sub>2</sub>Mn<sub>2</sub>O<sub>7</sub>, the calculated crystal sizes were decreased to nearly the value for pure Bi<sub>2</sub>Mn<sub>2</sub>O<sub>7</sub>.

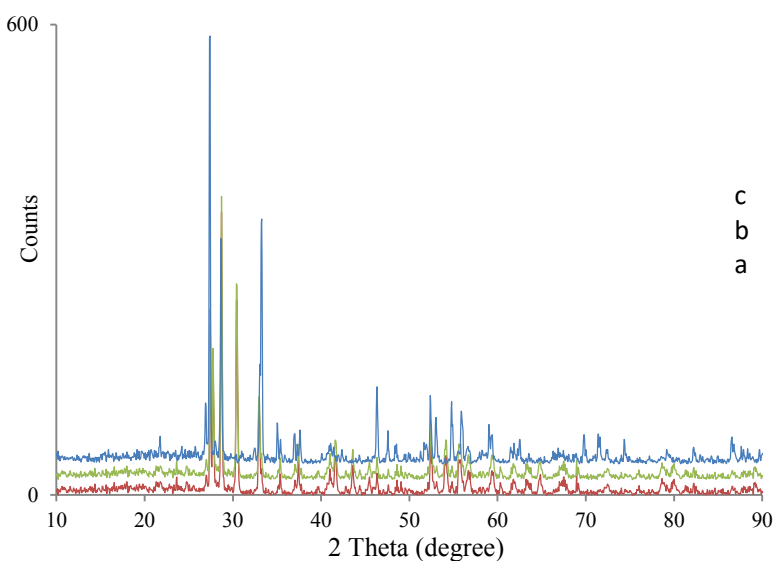


Fig. 1. PXRD patterns of Bi<sub>2-x</sub>La<sub>x</sub>Mn<sub>2</sub>O<sub>7</sub>. (a) x = 0.01(S<sub>1</sub>), (b) x = 0.02 (S<sub>2</sub>), and (c) x = 0.03.

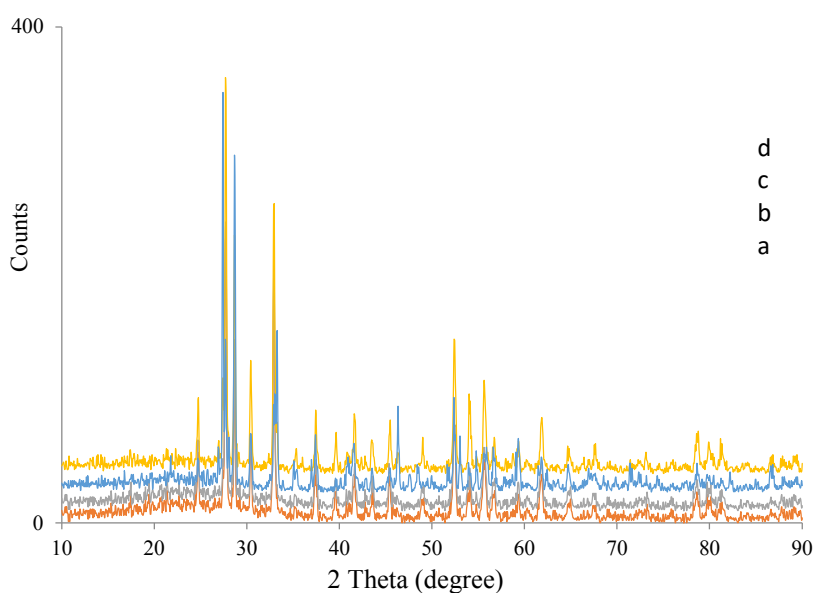


Fig. 2. PXRD patterns of  $Bi_{2-x}Sm_xMn_2O_7$ . (a)  $x = 0.01$  ( $S_3$ ), (b)  $x = 0.02$  ( $S_4$ ), (c)  $x = 0.03$  ( $S_5$ ), and (d)  $x = 0.04$ .

Table 1. Interplanar spacing (d) and cell parameter refinement data for pure and doped -  $Bi_2Mn_2O_7$  nanomaterials.

|                            | $Bi_2Mn_2O_7$ | $S_1$          | $S_2$           | $S_3$          | $S_4$           | $S_5$           |
|----------------------------|---------------|----------------|-----------------|----------------|-----------------|-----------------|
| $2\theta$ (°)              | 28.580        | 28.76          | 28.50           | 28.73          | 28.49           | 28.59           |
| d (Å)                      | 3.114         | 3.101          | 3.13            | 3.105          | 3.13            | 3.12            |
| a (SD)(Å)                  | 10.32501      | 10.3041(0.083) | 10.3311(0.0386) | 10.3176(0.077) | 10.3401(0.0667) | 10.3244(0.0492) |
| Vol. (SD)(Å <sup>3</sup> ) | 1100.71       | 1094.03(8.854) | 1102.64 (4.12)  | 1098.33(8.32)  | 1105.53 (7.12)  | 1100.52 (5.24)  |

Table 2. Scherrer data information for pure and doped -  $Bi_2Mn_2O_7$  nanomaterials.

| Data          | $2\theta$ | $\theta$ value | $B_{1/2}$ (°) | $B_{1/2}$ (rad) | $\cos\theta_B$ | t(nm) |
|---------------|-----------|----------------|---------------|-----------------|----------------|-------|
| $Bi_2Mn_2O_7$ | 28.58     | 14.290         | 0.217         | 0.00379         | 0.96910        | 37.7  |
| $S_1$         | 28.76     | 14.380         | 0.106         | 0.00185         | 0.96867        | 77.3  |
| $S_2$         | 28.50     | 14.250         | 0.111         | 0.00194         | 0.96923        | 73.7  |
| $S_3$         | 28.73     | 14.365         | 0.117         | 0.00204         | 0.96873        | 70.1  |
| $S_4$         | 28.49     | 14.245         | 0.185         | 0.00323         | 0.96925        | 44.3  |
| $S_5$         | 28.59     | 14.295         | 0.185         | 0.00323         | 0.96904        | 44.3  |

### Elemental analysis

The EDX spectra of the obtained nanomaterials as a function of  $La_2O_3$  and  $Sm_2O_3$  concentrations are presented in Fig. 3 a and b. The spectra indicated the X-rays emitted from various

elements. The peaks corresponding to La, Sm, Bi, Mn, and O atoms present in the sample are labeled. The respective energy positions and the specific X-ray lines from various elements are also indicated. The Figs illustrated the EDX

analyses for the sample doped with 0.02 and 0.03 mmol of  $\text{La}_2\text{O}_3$  and  $\text{Sm}_2\text{O}_3$ , respectively, which verify the doping and the compositional analysis of  $\text{La}^{3+}$  and  $\text{Sm}^{3+}$  in  $\text{Bi}_2\text{Mn}_2\text{O}_7$  nanomaterial. The normalized elemental analyses of the doped materials were 1.79 wt. % for  $\text{La}^{3+}$  and 2.84 wt. % for  $\text{Sm}^{3+}$ .

#### Microstructure analysis

Typical FESEM images recorded from  $\text{La}^{3+}$ -doped  $\text{Bi}_2\text{Mn}_2\text{O}_7$  nanomaterials are shown in Fig. 4 and 5. From the FESEM images in Fig. 4a–b, with the magnification of 30,000 $\times$ , and 60,000 $\times$ , respectively, it was obvious that the morphologies of the obtained materials were mainly rod-like,

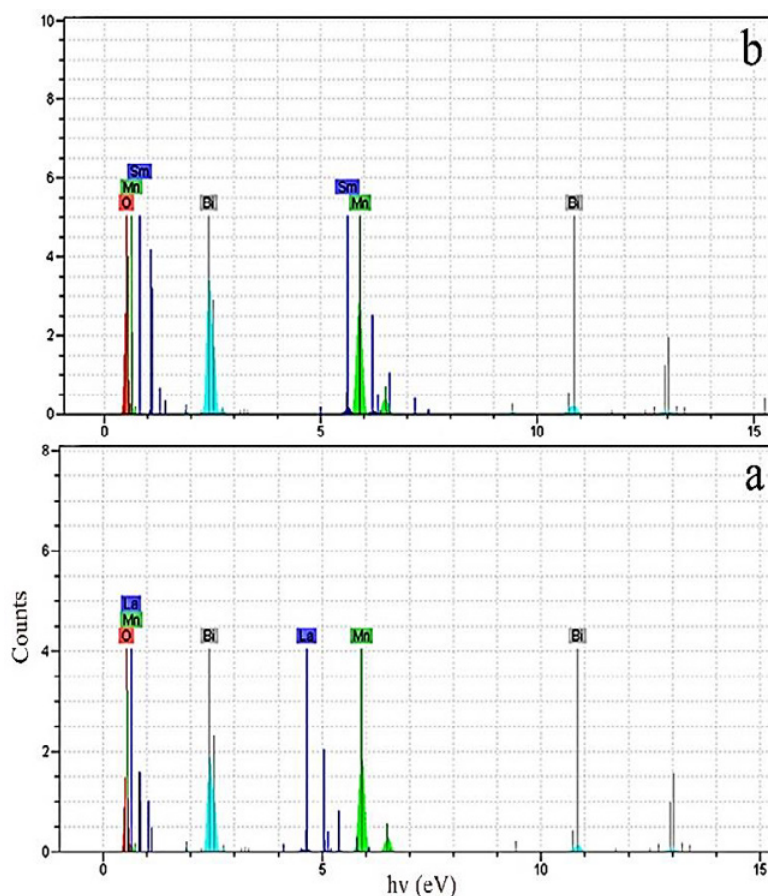


Fig. 3. EDX spectra of a)  $S_2$  and b)  $S_5$ .

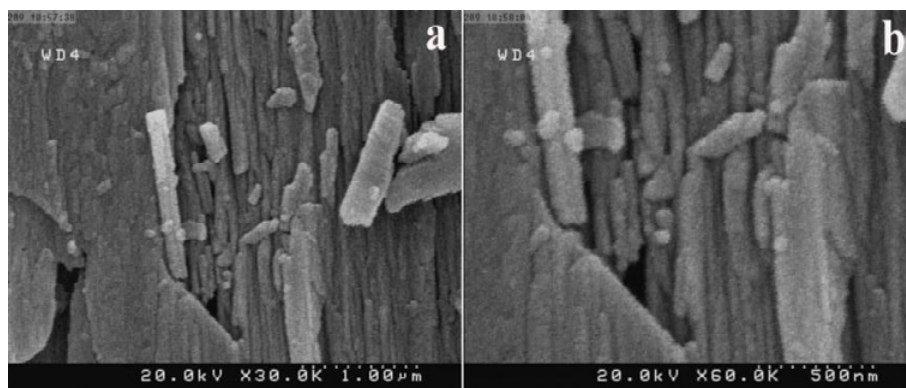


Fig. 4. FESEM images of  $S_1$ .

and some particles were present on the surface of the rods. At higher magnification of 60,000 $\times$  in Fig. 4b, it was clear that the thickness sizes of the rods were about 100 nm and the particles diameter sizes were about 50 nm.

Fig. 5 a and b with the magnifications of 30,000 $\times$ , and 100,000 $\times$  show that with increasing the dopant amount, the morphologies of the doped nanomaterials did not change considerably but the thickness size of the rods was decreased to about 60 nm and the particles' diameter sizes were about 30 – 60 nm.

FESEM images of  $\text{Sm}^{3+}$ -doped  $\text{Bi}_2\text{Mn}_2\text{O}_7$  nanomaterials are shown in Fig. 6, Fig. 7 and Fig.8. Fig. 6 a – b with the magnifications of 30,000 $\times$ , 60,000 $\times$ , and 90,000 $\times$  showed that the obtained nanomaterials had wire and rod-like morphologies. Fig. 6 b shows that the thickness sizes of the rod structures were about 70 nm and the length size was about 250 nm. It shows that the thickness sizes of the wires were about 70 nm and the length sizes were about 1.5  $\mu\text{m}$ .

Fig. 7 a – d with the magnifications of 4,000 $\times$ ,

6,000 $\times$ , 6,000 $\times$  and 20,000 $\times$  show that the morphology of the  $\text{S}_4$  was a mixture of prism and flower-like structures. It was clear that with increasing the dopant amount, the morphology was changed from wire and rod to flower structures. It seemed that the flower had been composed of some prisms that joined together and formed a flower structure. It was clear that the flowers thickness sizes were in micrometer ranges and were about 2 $\mu\text{m}$ . Fig. 7 a and d show that there are two kinds of prisms in view of their sizes. The length sizes of the larger prisms were about 15  $\mu\text{m}$  and for the smaller ones were about 1.5  $\mu\text{m}$ .

Fig. 8 a – d with the magnifications of 2,000 $\times$ , 10,000 $\times$ , 15,000 $\times$ , and 60,000 $\times$  show that the morphologies of the obtained nanomaterials were a mixture of prisms, wires and rod-like structures. It was found that there were some prisms that had been grown on the surface of the larger ones. It was also clear that there were some particles with rod-like morphologies on the surface of the prisms. Fig. 8d shows the wire and rod structures

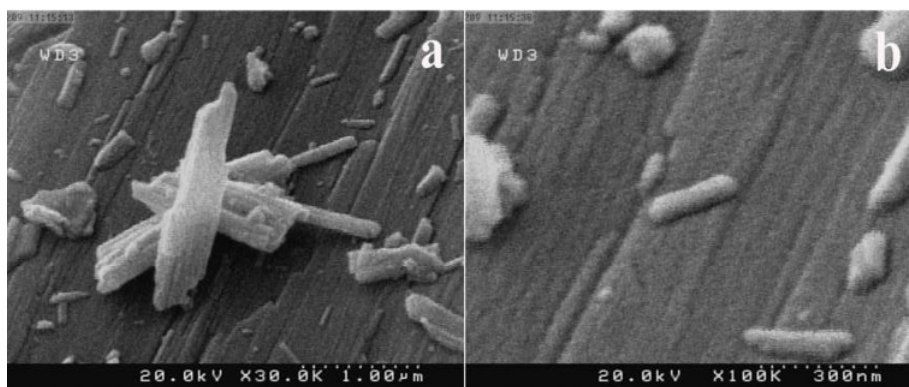


Fig. 5. FESEM images of  $\text{S}_2$ .

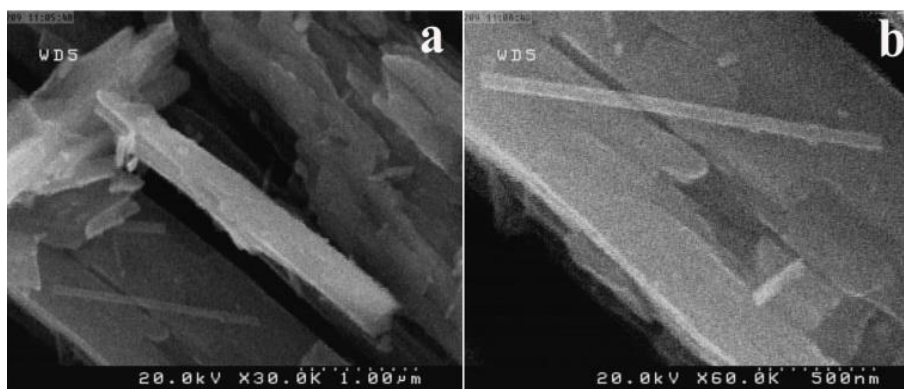


Fig. 6. FESEM images of  $\text{S}_3$ .

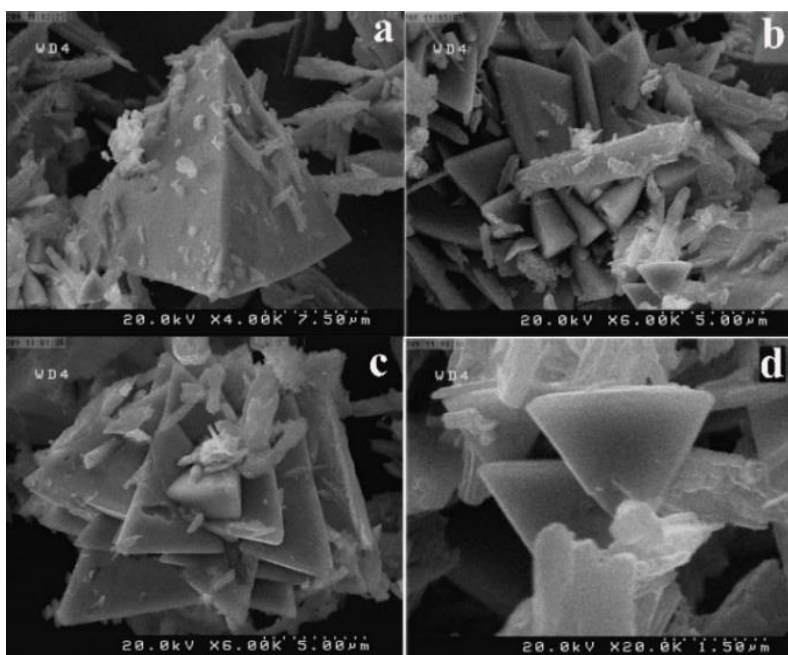


Fig. 7. FESEM images of  $\text{S}_4$ .

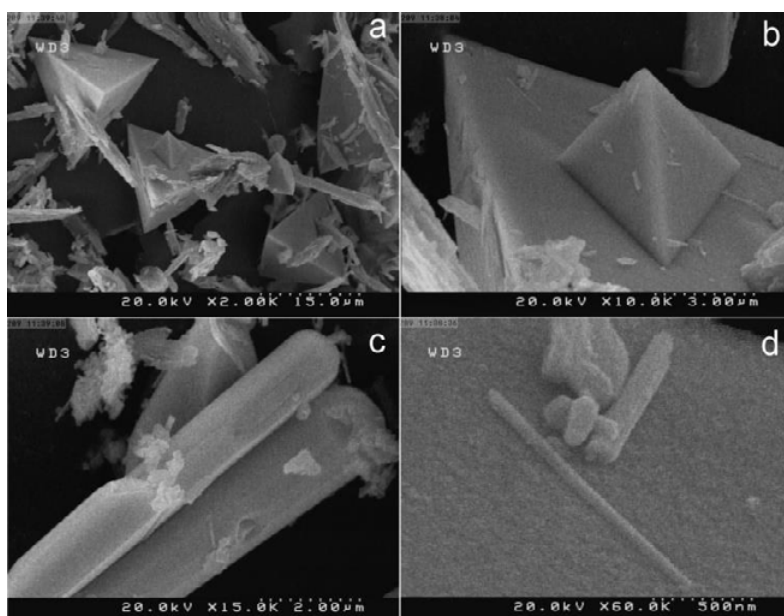


Fig. 8. FESEM images of  $\text{S}_5$ .

in one view. This figure shows that the wires thickness sizes were about 60 nm and the length sizes were about 1.5  $\mu\text{m}$ . Also, the rod thickness sizes were about 200 nm and the length sizes were about 1  $\mu\text{m}$ .

#### Optical property

The direct optical band gaps for pure  $\text{Bi}_2\text{Mn}_2\text{O}_7$ ,

and  $\text{La}^{3+}$  and  $\text{Sm}^{3+}$  doped  $\text{Bi}_2\text{Mn}_2\text{O}_7$  nanomaterials are shown in Fig. 9 a-c. To calculate the optical band gaps, we changed transmittance data to absorption ones using  $A = -\log(T/100)$  formula; where A is absorption and T is transmittance. According to the results of Pascual et al. [46], the relation between the absorption coefficient and incident photon energy can be written as  $(\alpha h\nu)^2 =$

$A(h\nu - E_g)$ , where  $A$  and  $E_g$  are constant and direct band gap energy, respectively. Band gap energies were evaluated by extrapolating the linear part of the curve to the energy axis. It was found that by doping  $\text{La}^{3+}$  and  $\text{Sm}^{3+}$  into  $\text{Bi}_2\text{Mn}_2\text{O}_7$ , the band gap was increased; i.e., 3.8 and 4.30 eV for  $\text{S}_2$ ; and 3.9 and 4.3 eV for  $\text{S}_5$ .

#### Catalytic studies

##### Biginelli reaction for the synthesis of DHPMs

The one-pot condensation between ketoesters, aldehydes and urea, in the presence of either Lewis or mineral acids, results in the synthesis of DHPMs. In this study, DHPMs were prepared from the condensation of aromatic aldehydes, ethyl acetoacetate in presence of 0.014 g of doped  $\text{Bi}_2\text{Mn}_2\text{O}_7$  ( $\text{S}_2$  and  $\text{S}_5$ ) at 104 °C for 66 min under

solvent free conditions (Fig. 10). The optimum conditions were used as for pure  $\text{Bi}_2\text{Mn}_2\text{O}_7$  [40]. The results are collected in table 3.

Table 4 shows the catalytic efficiency of the synthesized doped  $\text{Bi}_2\text{Mn}_2\text{O}_7$  nanomaterials compared to that of pure  $\text{Bi}_2\text{Mn}_2\text{O}_7$  [40]. The optimized conditions from the previous work were used [40]. In two earlier works, we have reported the catalytic efficiency of  $\text{Bi}_2\text{Mn}_2\text{O}_7$  and  $\text{Bi}_2\text{V}_2\text{O}_7$  nanomaterials in the Biginelli reactions [6, 40]. In those works, we concluded that the band gap had an important effect on the catalytic performance of the studied nanomaterials.  $\text{Bi}_2\text{V}_2\text{O}_7$  with the lower band gap was the more efficient catalyst. Another conclusion which was drawn was that the hard and soft nature of the metal ions was also important.  $\text{Bi}_2\text{V}_2\text{O}_7$  with the slightly softer  $\text{V}^{4+}$

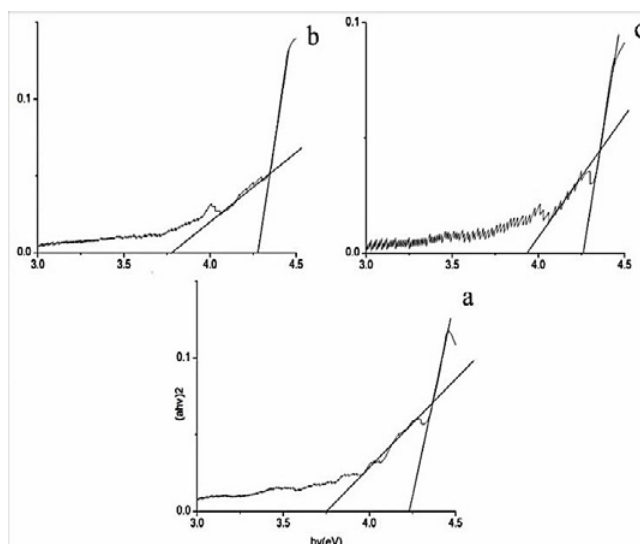


Fig. 9. Plots of  $(\alpha hv)^2$  versus  $h\nu$  for (a)  $\text{Bi}_2\text{Mn}_2\text{O}_7$ , (b)  $\text{S}_2$  and (c)  $\text{S}_5$ .

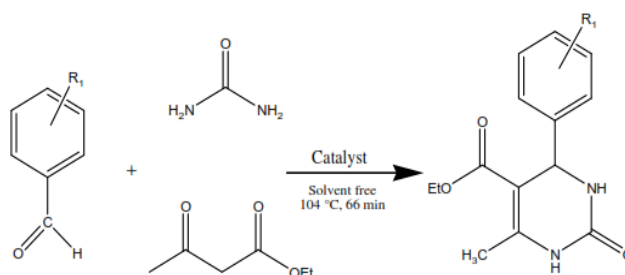


Fig. 10. Schematic representation of the reaction pathway for the synthesis of DHPMs.

Table 3. Biginelli reactions using ethyl acetoacetate and urea with different benzaldehyde derivatives.

| R                 | Yield (%) of products for: |                |                |                |                |
|-------------------|----------------------------|----------------|----------------|----------------|----------------|
|                   | S <sub>1</sub>             | S <sub>2</sub> | S <sub>3</sub> | S <sub>4</sub> | S <sub>5</sub> |
| H                 | 89                         | 92             | 85             | 92             | 85             |
| 4-Cl              | 47                         | 51             | 34             | 41             | 37             |
| 2-Cl              | 75                         | 78             | 71             | 78             | 71             |
| 3-OMe             | 40                         | 44             | 62             | 44             | 55             |
| 3-OH              | 94                         | 91             | 94             | 83             | 76             |
| 3-NO <sub>2</sub> | 92                         | 85             | 95             | 92             | 88             |

Table 4. Comparison study of the catalytic ability among the synthesized doped  $\text{Bi}_2\text{Mn}_2\text{O}_7$  nanomaterial and pure  $\text{Bi}_2\text{Mn}_2\text{O}_7$ .

| Catalyst                           | Band gap (eV) | H  | 4-Cl | 2-Cl |
|------------------------------------|---------------|----|------|------|
| $\text{Bi}_2\text{Mn}_2\text{O}_7$ | 3.75 and 4.20 | 96 | 89   | 86   |
| S <sub>2</sub>                     | 3.80 and 4.30 | 92 | 51   | 78   |
| S <sub>5</sub>                     | 3.90 and 4.30 | 85 | 37   | 71   |

Table 5. Comparison study of the catalytic ability of the synthesized doped  $\text{Bi}_2\text{Mn}_2\text{O}_7$  nanocatalysts with other catalysts.

| Catalyst   | R <sub>1</sub> | Catalyst amount           | Reaction Condition      | Yield % | Time (min) | Ref.      |
|--|----------------|---------------------------|-------------------------|---------|------------|-----------|
| S <sub>2</sub>   | H              | 0.014 g                   | solvent-free, 104 °C    | 92      | 66         | This work |
|  | 4-Cl           |                           |                         | 51      |            |           |
|  | 2-Cl           |                           |                         | 78      |            |           |
| S <sub>5</sub>   | H              | 0.014 g                   | solvent-free, 104 °C    | 82      | 66         | This work |
|  | 4-Cl           |                           |                         | 37      |            |           |
|  | 2-Cl           |                           |                         | 71      |            |           |
| $\text{Bi}_2\text{V}_2\text{O}_7$                          | H              | $3.1 \times 10^{-2}$ mmol | solvent-free, 90 °C     | 89      | 60         | [6]       |
|  | 4-Cl           |                           |                         | 92      |            |           |
|  | 2-Cl           |                           |                         | 98      |            |           |
| $\text{ZrO}_2\text{-Al}_2\text{O}_3\text{-Fe}_3\text{O}_4$ | H              | 0.05 g                    | Ethanol, reflux, 140 °C | 82      | 300        | [32]      |
|  | 4-Cl           |                           |                         | 66      |            |           |
|  | 2-Cl           |                           |                         | 40      |            |           |
| $\text{Mo}/\gamma\text{-Al}_2\text{O}_3$                   | H              | 0.3 g                     | solvent-free at 100 °C  | 80      | 60         | [34]      |
| ZnO  | H              | 25 mol%                   | solvent-free at 90 °C   | 92      | 50         | [36]      |
|  | 4-Cl           |                           |                         | 95      |            |           |
| $\text{Bi}_2\text{O}_3/\text{ZrO}_2$                       | H              | 20 mol%                   | solvent-free, 80-85 °C  | 85      | 120        | [37]      |
|  | 4-Cl           |                           |                         | 85      | 120        |           |
|  | 2-Cl           |                           |                         | 82      | 165        |           |
| $\text{Bi}_2\text{Mn}_2\text{O}_7$                         | H              | $2.2 \times 10^{-2}$ mmol | solvent-free, 104 °C    | 96      | 66         | [40]      |
|  | 4-Cl           |                           |                         | 89      |            |           |
|  | 2-Cl           |                           |                         | 86      |            |           |

compared to  $\text{Mn}^{4+}$  in  $\text{Bi}_2\text{Mn}_2\text{O}_7$  had shown better catalytic performance. To further confirm this idea we prepared  $\text{La}^{3+}$  and  $\text{Sm}^{3+}$  doped  $\text{Bi}_2\text{Mn}_2\text{O}_7$ . Our results collected in table 4 shows that by doping the  $\text{M}^{3+}$  metal ions into  $\text{Bi}_2\text{Mn}_2\text{O}_7$ , the band gap was increased. The increased band gap has resulted in the decreased catalytic performance of the synthesized nanomaterials in Biginelli reactions. It could also be concluded that since the harder  $\text{M}^{3+}$  ions have replaced the softer  $\text{Bi}^{3+}$  metal ion, the catalytic performance was also decreased.

To show the merit of the present work, we

have compared the doped  $\text{Bi}_2\text{Mn}_2\text{O}_7$  nanocatalysts results with some of the previously reported catalysts in the synthesis of DHPMs (table 5). It is clear that the doped  $\text{Bi}_2\text{Mn}_2\text{O}_7$  nanocatalysts showed greater activity than some other heterogeneous catalysts.

## CONCLUSION

In this work,  $\text{La}^{3+}$  and  $\text{Sm}^{3+}$  - doped  $\text{Bi}_2\text{Mn}_2\text{O}_7$  nanomaterials were synthesized via a mild condition hydrothermal method. The catalytic application of the synthesized nanomaterials was

investigated in Biginelli reaction in solvent free conditions. It was found that the doped-Bi<sub>2</sub>Mn<sub>2</sub>O<sub>7</sub> nanocatalysts had considerable efficiency in the synthesis of DHPMs. A correlation between the band gap results and the hard/soft nature of the metal ions was concluded.

### CONFLICT OF INTEREST

The authors declare that there are no conflicts of interest regarding the publication of this manuscript.

### REFERENCE

1. Radhakrishnan AN, Rao PP, Linsa KSM, Deepa M, Koshy P. Influence of disorder-to-order transition on lattice thermal expansion and oxide ion conductivity in (Ca<sub>x</sub>Gd<sub>1-x</sub>)<sub>2</sub>(Zr<sub>1-x</sub>Mx)<sub>2</sub>O<sub>7</sub> pyrochlore solid solutions. *Dalton Transactions*. 2011;40(15): 3763-3839.
2. Blanchard PER, Liu S, Kennedy BJ, Ling CD, Zhang Z, Avdeev M, et al. Investigating the order-disorder phase transition in Nd<sub>2-x</sub>YxZr<sub>2</sub>O<sub>7</sub> via diffraction and spectroscopy. *Dalton Transactions*. 2013;42(41):14875.
3. Martínez-Coronado R, Retuerto M, Fernández MT, Alonso JA. Evolution of the crystal and magnetic structure of the R<sub>2</sub>MnRuO<sub>7</sub> (R = Tb, Dy, Ho, Er, Tm, Yb, Lu, and Y) family of pyrochlore oxides. *Dalton Transactions*. 2012;41(28):8575.
4. Sickafus KE, Minervini L, Grimes RW, Valdez JA, Ishimaru M, Li F, McClellan KJ, Hartmann T. Radiation Tolerance of Complex Oxides. *Science*, 2000; 289 (5480): 748-751.
5. Sickafus KE. Radiation Tolerance of Complex Oxides. *Science*. 2000;289(5480):748-51.
6. Khademinia S, Behzad M, Jahromi HS. Solid state synthesis, characterization, optical properties and cooperative catalytic performance of bismuth vanadate nanocatalyst for Biginelli reactions. *RSC Advances*. 2015;5(31):24313-8.
7. Khademinia S, Behzad M. hydrothermal synthesis, characterization and optical properties of strontium pyroniobate. *Adv. Powder Tech.*, 2015; 26 (2): 644-649.
8. Khademinia S, Behzad M. Low temperature hydrothermal synthesis, characterization and optical properties of strontium pyroniobate. *Advanced Powder Technology*. 2015;26(2):644-9.
9. Khademinia S, Behzad M. Lanthanum cerate (La<sub>2</sub>Ce<sub>2</sub>O<sub>7</sub>): hydrothermal synthesis, characterization and optical properties. *International Nano Letters*. 2015;5(2):101-7.
10. Jones A, Slater PR, Islam MS. Local Defect Structures and Ion Transport Mechanisms in the Oxygen-Excess Apatite La<sub>9.67</sub>(SiO<sub>4</sub>)<sub>6</sub>O<sub>2.5</sub>. *Chemistry of Materials*. 2008;20(15):5055-60.
11. Qin C, Huang Y, Chen G, Shi L, Qiao X, Gan J, et al. Luminescence properties of a red phosphor europium tungsten oxide Eu<sub>2</sub>WO<sub>6</sub>. *Materials Letters*. 2009;63(13-14):1162-4.
12. Cavalli E, Calestani G, Belletti A, Bettinelli M, Speghini A. Optical spectroscopy of Nd<sup>3+</sup> in LiLa<sub>9</sub>(SiO<sub>4</sub>)<sub>6</sub>O<sub>2</sub> crystals. *Optical Materials*. 2009;31(9):1340-2.
13. Yang Z, Tian J, Wang S, Yang G, Li X, Li P. Combustion synthesis of SrIn<sub>2</sub>O<sub>4</sub>:Eu<sup>3+</sup> red-emitting phosphor for white light-emitting diodes. *Materials Letters*. 2008;62(8-9):1369-71.
14. Zhang W, Lu C, Ni Y, Song J, Xu Z. Preparation and characterization of Sm<sub>2</sub>O<sub>3</sub>/Cu mosaic structure with infrared absorptive properties and low infrared emissivity. *Materials Letters*. 2012;87:13-6.
15. Khor KA, Yang J. Lattice parameters, tetragonality (t) and transformability of tetragonal zirconia phase in plasma-sprayed ZrO<sub>2</sub>-Er<sub>2</sub>O<sub>3</sub> coatings. *Materials Letters*. 1997;31(1-2):23-7.
16. Belous AG, Kravchik KV, Pashkova EV, Bohnke O, Galven C. Influence of the Chemical Composition on Structural Properties and Electrical Conductivity of Y-Ce-ZrO<sub>2</sub>. *Chemistry of Materials*. 2007;19(21):5179-84.
17. Bukaemskiy AA, Barrier D, Modolo G. Physical properties of 8mol% Ceria doped yttria stabilised zirconia powder and ceramic and their behaviour during annealing and sintering. *Journal of the European Ceramic Society*. 2006;26(8):1507-15.
18. Kaplyanskiĭ AA, Kulinkin AB, Kutsenko AB, Feofilov SP, Zakharchenya RI, Vasilevskaya TN. Optical spectra of triply-charged rare-earth ions in polycrystalline corundum. *Physics of the Solid State*. 1998;40(8):1310-6.
19. Alemi A, Khademinia S. Part I: lithium metasilicate (Li<sub>2</sub>SiO<sub>3</sub>)—mild condition hydrothermal synthesis, characterization, and optical properties. *International Nano Letters*. 2014;5(1):15-20.
20. Nogami M, Abe Y. Properties of sol-gel-derived Al<sub>2</sub>O<sub>3</sub>-SiO<sub>2</sub> glasses using Eu<sup>3+</sup> ion fluorescence spectra. *Journal of Non-Crystalline Solids*. 1996;197(1):73-8.
21. Khademinia S, Behzad M. Bismuth Pyromanganate: Hydrothermal and Solid State Synthesis, Characterization and Optical Properties. *J. Adv. Mater. Proc.*, 2015; 3 (1): 77-84.
22. Khademinia S, Behzad M, Jahromi HS. Solid state synthesis, characterization, optical properties and cooperative catalytic performance of bismuth vanadate nanocatalyst for Biginelli reactions. *RSC Advances*. 2015;5(31):24313-8.
23. Biginelli P. Ueber Aldehyduramide des Acetessigäthers. *Berichte der deutschen chemischen Gesellschaft*. 1891;24(1):1317-9.
24. Genesis of Dihydropyrimidinone Calcium Channel Blockers: Recent Progress in Structure-Activity Relationships and Other Effects. *Mini-Reviews in Medicinal Chemistry*. 2009;9(1):95-106.
25. Kouachi K, Lafaye G, Pronier S, Bennini L, Menad S. Mo/γ-Al<sub>2</sub>O<sub>3</sub> catalysts for the Biginelli reaction. Effect of Mo loading. *Journal of Molecular Catalysis A: Chemical*. 2014;395:210-6.
26. Tamaddon F, Moradi S. Controllable selectivity in Biginelli and Hantzsch reactions using nanoZnO as a structure base catalyst. *Journal of Molecular Catalysis A: Chemical*. 2013;370:117-22.
27. Samantaray S, Mishra BG. Combustion synthesis, characterization and catalytic application of MoO<sub>3</sub>-ZrO<sub>2</sub> nanocomposite oxide towards one pot synthesis of octahydroquinazolinones. *Journal of Molecular Catalysis A: Chemical*. 2011;339(1-2):92-8.
28. Safari J, Gandomi-Ravandi S. MnO<sub>2</sub>-MWCNT nanocomposites as efficient catalyst in the synthesis of Biginelli-type compounds under microwave radiation. *Journal of Molecular Catalysis A: Chemical*. 2013;373:72-7.
29. Memarain HR, Ranjbar M. Substituent effect in photocatalytic oxidation of 2-oxo-1,2,3,4-tetrahydropyrimidines using TiO<sub>2</sub> nanoparticles. *Journal of Molecular Catalysis A:*

- Chemical. 2012;356:46-52.
30. Guguloth VC, Raju G, Basude M, Battu S. Efficient, stable and reusable  $\text{Bi}_2\text{O}_3/\text{ZrO}_2$  catalyzed one-pot synthesis of 3, 4-dihydropyrimidin-2 (1H)-ones under solvent-free conditions. *Int. J. Chem. Anal. Sci.*, 2014; 5(2): 86-92.
  31. Ahmed N, van Lier JE. TaBr5-catalyzed Biginelli reaction: one-pot synthesis of 3,4-dihydropyrimidin-2-(1H)-ones/thiones under solvent-free conditions. *Tetrahedron Letters*. 2007;48(31):5407-9.
  32. Wang A, Liu X, Su Z, Jing H. New magnetic nanocomposites of  $\text{ZrO}_2\text{-Al}_2\text{O}_3\text{-Fe}_3\text{O}_4$  as green solid acid catalysts in organic reactions. *Catal Sci Technol*. 2014;4(1):71-80.
  33. Javidi J, Esmailpour M, Dodeji FN. Immobilization of phosphomolybdic acid nanoparticles on imidazole functionalized  $\text{Fe}_3\text{O}_4@\text{SiO}_2$ : a novel and reusable nanocatalyst for one-pot synthesis of Biginelli-type 3,4-dihydro-pyrimidine-2-(1H)-ones/thiones under solvent-free conditions. *RSC Advances*. 2015;5(1):308-15.
  34. Jain SL, Prasad VVDN, Sain B. Alumina supported  $\text{MoO}_3$ : An efficient and reusable heterogeneous catalyst for synthesis of 3,4-dihydropyridine-2(1H)-ones under solvent free conditions. *Catalysis Communications*. 2008;9(4):499-503.
  35. Pourshamsian Kh. ZnO-NPs as an efficient reusable heterogeneous catalyst for synthesis of 1,4-Dihydropyrimidine derivatives in solvent-free conditions. *Int. J. Nano Dimens.*, 2015; 6 (1): 99-104.
  36. An efficient one-pot synthesis of polyhydroquinoline derivatives via Hantzsch condensation using heterogeneous catalyst under solvent-free conditions. *Arkivoc*. 2006;2006(2):201.
  37. Safari J, Gandomi-Ravandi S.  $\text{Fe}_3\text{O}_4\text{-CNTs}$  nanocomposites: a novel and excellent catalyst in the synthesis of diarylpyrimidinones using grindstone chemistry. *RSC Adv*. 2014;4(22):11486-92.
  38. Safari J, Gandomi-Ravandi S. Titanium dioxide supported on MWCNTs as an eco-friendly catalyst in the synthesis of 3,4-dihydropyrimidin-2-(1H)-ones accelerated under microwave irradiation. *New J Chem*. 2014;38(8):3514-21.
  39. Mondal J, Sen T, Bhaumik A.  $\text{Fe}_3\text{O}_4$ @mesoporous SBA-15: a robust and magnetically recoverable catalyst for one-pot synthesis of 3,4-dihydropyrimidin-2(1H)-ones via the Biginelli reaction. *Dalton Transactions*. 2012;41(20):6173.
  40. Soleimani F, Behzad M, Salehi M. experimentally designed optimized conditions for catalytic performance of nanostructured  $\text{RuO}_2$  in Biginelli reaction. *JNS.*, 2015: 5 (4): 351-360.
  41. Bahari A, Khorshidi Z, Gholipur R. Proceedings of the 4th International Conference on Nanostructures (ICNS4) 12-14 March, 2012, Kish Island, I.R. Iran.
  42. Bahari A, Gholipur R, Khorshidi Z. Electrical Properties of Zr-Doped  $\text{La}_2\text{O}_3$  Nanocrystallites as a Good Gate Dielectric. *Defect and Diffusion Forum*. 2012;329:129-38.
  43. Méndez M, Carvajal JJ, Cesteros Y, Aguiló M, Díaz F, Giguère A, et al. Sol-gel Pechini synthesis and optical spectroscopy of nanocrystalline  $\text{La}_2\text{O}_3$  doped with  $\text{Eu}^{3+}$ . *Optical Materials*. 2010;32(12):1686-92.
  44. Park DJ, Sekino T, Tsukuda S, Hayashi A, Kusunose T, Tanaka S-I. Photoluminescence of samarium-doped  $\text{TiO}_2$  nanotubes. *Journal of Solid State Chemistry*. 2011;184(10):2695-700.
  45. Zhang H, Dai H, Liu Y, Deng J, Zhang L, Ji K. Surfactant-mediated PMMA-templating fabrication and characterization of three-dimensionally ordered macroporous  $\text{Eu}_2\text{O}_3$  and  $\text{Sm}_2\text{O}_3$  with mesoporous walls. *Materials Chemistry and Physics*. 2011;129(1-2):586-93.
  46. Pascual J, Camassel J, Mathieu H. Fine structure in the intrinsic absorption edge of  $\text{TiO}_2$ . *Physical Review B*. 1978;18(10):5606-14.